Biomass burning organic aerosol (BBOA) from wildfires has multiple phases and is more viscous than laboratory generated BBOA

Nealan G. A. Gerrebos,[1] Julia Zaks,[1] Florence K. A. Gregson,[1§] Max Walton-Raaby,[2†] Harrison Meeres,[3‡] Ieva Zigg,[3] Wesley F. Zandberg,[3] Allan K. Bertram[1]*

Author affiliations:
[1] Department of Chemistry, University of British Columbia, Vancouver, British Columbia V6T 1Z1, Canada
[2] Department of Chemistry, Thompson Rivers University, Kamloops, British Columbia V2C 0C8, Canada
[3] Department of Chemistry, University of British Columbia-Okanagan, Kelowna, British Columbia V1V 1V7, Canada
* bertram@chem.ubc.ca
§Current Address: STEMCELL Technologies, 1618 Station St, Vancouver, BC V6A 1B6, Canada
†Current Address: University of Waterloo, 200 University Ave W, Waterloo, ON N2L 3G1, Canada
‡Current Address: TRIUMF, 4004 Wesbrook Mall, Vancouver, BC V6T 2A3, Canada

Abstract

Biomass burning organic aerosol (BBOA) is a major contributor to organic aerosol in the atmosphere. The impacts of BBOA on climate and health depend strongly on their physicochemical properties, including viscosity and phase behaviour (number and types of phases); these properties, and their relationships to BBOA chemistry, are not yet fully characterized. We collected BBOA field samples during the 2021 British Columbia wildfire season to constrain the viscosity and phase behaviour at a range of relative humidities, and compared them to laboratory generated BBOA made from smoldering pine wood. Particles from all samples exhibited two-phased behaviour with a higher polarity hydrophilic core and a lower polarity hydrophobic shell. We used the poke-flow viscosity technique to estimate the viscosity of the particles. We found that both phases of the field samples had viscosities $>10^8$ Pa s at relative humidities up to 50%, which is more viscous than any laboratory generated BBOA or BBOA proxies previously measured. Aerosol mass spectrometry showed that the field samples were more oxidized than those generated in the lab, which is a likely explanation for the higher viscosity. The two phases and high viscosity have implications for how BBOA should be treated in atmospheric models.

Keywords

Biomass burning, organic aerosol, viscosity, phase behaviour, phase separation

Synopsis

Research on the physical properties of biomass burning aerosol is lacking. This study compares the viscosity and phase behaviour of forest fire smoke from the field and the lab.

Introduction

Aerosols, small liquid or solid particles suspended in the air, are found throughout the troposphere and originate from both anthropogenic (e.g. vehicle exhaust) and natural sources (e.g. wildfires). Biomass burning is a significant contributor to aerosol concentrations in most regions of the world.[1–8] Smoke from biomass burning consists of mostly organic aerosol, referred to as biomass-burning organic aerosol (BBOA).[9] For example, smoke sampled from wildfires in the western U.S.A. consisted of > 90% BBOA.[10,11] As climate change continues, the frequency and intensity of wildfires is increasing in many regions due to rising temperatures and changing precipitation patterns.[12–15] This should cause the portion of aerosols attributed to biomass burning to grow.

BBOA can cause negative health effects.[1,16–19] In addition, BBOA contains light absorbing molecules known as brown carbon (BrC) that warm the climate by absorbing sunlight.[20,21,21–24] BBOA also acts as nuclei for liquid cloud droplets and possibly ice clouds, thereby indirectly modifying the climate.[25–27]

Viscosity and phase behavior (number and types of phases) influence the role of BBOA particles in air quality and climate. For example, if a BBOA particle contains two phases then the equilibrium partitioning of gas phase species into the particles is changed compared to the non-phase separated case, which impacts how the particles grow and gain mass – in turn influencing their health and climate impacts.[28–30] The presence of two non-crystalline phases has also been shown to change cloud condensation nuclei activity.[31–33] Compared to a well-mixed droplet, a phase-separated droplet with a low polarity organic outer phase has lower surface tension, which lowers the barrier to cloud condensation.[33] If the BBOA particles are sufficiently viscous, the viscosity could limit reactions within the particles by limiting intra-particle diffusion rates.[34–41] Furthermore, if BBOA particles have a viscosity $> 10^{12}$ Pa s (i.e. the particles are in a glassy state), they may be good nuclei for crystalline ice and influence the properties and frequency of ice clouds.[26]

Several studies have directly or indirectly determined the viscosity of BBOA generated in the laboratory. For example, Schnitzler et al. reported the viscosity of water-soluble BBOA extracts from smoldered pine wood.[37] Gregson et al. reported diffusion rates within both phases of core-shell particles of BBOA from smoldering pine wood.[34] Kiland et al. reported the viscosity of chamber secondary organic aerosol generated from biomass burning-like phenolic volatile organic compounds.[42] Xu et al. investigated the glass transition temperatures of BBOA from straw and wood burning before and after photochemical aging in an oxidative flow reactor.[42]

Only a few studies have focused on the phase behavior of BBOA. Gregson et al. observed two phases over a wide range of relative humidity (RH) values in BBOA.[34] Jahn et al. observed particles from sawgrass BBOA, and some particles displayed two organic phases under dry conditions in a vaccum.[44] Hettiyadura et al. and Li et al. have both shown that tar condensates from both burning and O_2-free pyrolysis of wood separate into immiscible aqueous and oily liquid phases.[45,46] Despite the above, models simulating the chemistry, transport, and climatic impacts of wildfire BBOA typically assume that BBOA comprises only a single phase.[37,47–49]

Our understanding of the viscosity and phase behaviour of BBOA remains incomplete, in part, because previous studies have focused on samples generated in the laboratory and not collected from the real atmosphere. The composition of BBOA in the real atmosphere may be different than the composition of BBOA in the laboratory for several reasons including atmospheric aging of BBOA, higher degrees of dilution, and burning conditions (e.g. fuel type, temperature, humidity, availability of oxygen). These factors could lead to atmospheric BBOA having a very different viscosity than what is assumed based on laboratory results, and phase behaviour may differ as well.[49,50] Particularly, phase separation has been explained as being driven by differences in polarity, approximated by the oxygen-to-carbon ratio (O:C).[51–56] Atmospheric aging increases O:C,[58,59] so atmospheric aging of particles could change their phase behaviour.

In the following, we investigated the viscosity and phase-behavior of BBOA samples generated from forest fire smoke samples collected in the real atmosphere. For comparison, we also investigated the viscosity and phase-behavior of BBOA generated by smoldering pine wood in the laboratory. Viscosity was probed with the poke-flow technique and phase-behavior was measured with optical microscopy. The results show that BBOA samples from forest fire smoke collected in the real atmosphere and in the lab from pine-smoldering always have two phases. We also found that the field collected BBOA samples are significantly more viscous than the lab-generated BBOA samples measured in both the current and previous studies.

Methods and Materials

Field BBOA Collection. Field BBOA was collected on 47 mm PTFE membrane filters (MTL, USA) at the University of British Columbia – Okanagan (Kelowna, Canada) and Thompson Rivers University (Kamloops, Canada) (see sample locations in Figure S1) in early August 2021 during heavy forest fire activity. Here we focus on two samples: one collected in Kelowna from August 3rd to August 6th and one collected in Kamloops from August 2nd to August 5th. $PM_{2.5}$ concentrations during the two sampling periods reached over 100 µm m^{-3}, according to British Columbia air quality monitoring stations located in the same cities as the collection sites (Figure S2). The air quality monitoring stations were approximately 10 km away in Kamloops and 2 km away in Kelowna. Data was acquired from the BC Air Data Archive Website.[60] In the first half of 2021, before the start of the wildfire season, the average $PM_{2.5}$ concentrations in Kelowna and Kamloops were 5.0 and 5.7 µg m^{-3}, respectively – up to 60 times less than during our wildfire-influenced sampling period (Figure S2). Therefore, any influence on phase behaviour by non-BBOA species should be minimal.

Satellite measurements show many forest fires surrounding Kamloops and Kelowna during sampling (Figure S1). Fire locations were gathered from the Fire Information for Resource Management System (FIRMS) U.S./Canada,[61] using data from VIIRS NOAA-20, VIIRS S-NPP, MODIS Aqua and MODIS Terra.

Forests in the burnt regions primarily consist of trees in the *Pinaceae* family, such as Douglas-fir and lodgepole pine.[62,63] Back trajectories suggest that the field samples contained smoke from fires of varying distance from the collection site and had an atmospheric age of approximately 12 hours or less (Figure S1). The back trajectories were run with the HYSPLIT transport and dispersion model on the READY website from NOAA Air Resources Laboratory (ARL).[64,65] Back trajectories were run once every 12 hours during the sampling period with a starting height of 0 m and using GFS meteorology (0.25 degrees, global).

For sampling, scroll pumps (Agilent, USA) were used to draw approximately 30 L min^{-1} through the filters until roughly 5 mg of PM$_{2.5}$ was collected on each filter. The mass on each filter was estimated based on PM$_{2.5}$ concentrations from the air quality monitoring stations located in the same cities as the collection sites (Figure S2) and daily in-line flow meter measurements (Mass Flow Meter 4043, TSI, USA).

Laboratory generated BBOA. BBOA was also collected in the lab by burning pine chips in a flow-tube furnace at smoldering temperatures, as in Gregson et al.,[34] with the exception of samples being collected on filters instead of glass slides. Briefly, 1.2 g of pine chips was placed in a quartz flow tube with 2 L min^{-1} of air flowing through it and heated to 400°C by a ceramic heater that fit around the tube (Watlow, USA). This caused the pine to smolder, and the resulting BBOA flowed into a 19 L glass vessel where it was subject to a 10:1 dilution, and then drawn out of the dilution vessel and through the same type of 47 mm PTFE filters used in field sampling.

Sample Preparation. BBOA field and laboratory filters were extracted with a 1/1 (v/v) solution of methanol (HPLC grade, Sigma-Aldrich)/water (HPLC grade, Thermo Scientific). Filters were cut into quarters and placed in glass vials into which 1.5 mL of solvent was added, and then shaken on a platform shaker at 200 rpm for 2 hours. Afterwards, the solutions were passed through 13 mm diameter, 0.45 µm pore Fluoropore membrane syringe filters (Millipore, USA) to remove soot and other insoluble components. Filtered extracts were stored in glass vials at 4°C and wrapped in aluminum foil to limit their exposure to light and avoid any photochemistry. Hems et al. and Trofimova et al. showed that water extracts 70-75% of unaged BBOA, while organic solvents including methanol are able to extract nearly 100% of unaged BBOA mass.[66,67] As BBOA is aged, the amount that can be extracted with water is expected to increase and the amount extracted with methanol may decrease as oxidation will increase BBOA's polarity. We therefore expect our extract to have recovered between 70 to 100% of the organic aerosol material from the filters.

Phase behaviour. Samples for phase behaviour experiments were prepared by nebulizing extracts of the field or laboratory samples onto 13 mm diameter glass slides coated with FluoroPel 800 (Cytonix, USA), a hydrophobic coating, to promote spherical droplet formation. Extracts were nebulized using a syringe pump and a pneumatic nebulizer (Part #G1946-67098, Agilent, USA) with a sheath gas flow of 15 L min^{-1} to dry the particles (Figure S3). The particles were then collected on the glass slides using a micro-orifice uniform deposit impactor (MOUDI-II 120, TSI,

USA) (Figure S3). After impaction, the slides were conditioned at 95% relative humidity (RH) overnight above a saturated KNO_3 solution in a sealed jar.[68] The high RH values allowed for the impacted particles to take up water and grow and take on more spherical shapes, which are better for imaging. To observe the phase behaviour, the slides were imaged at relative humidity values ranging from 0-100% within an RH-controlled flow cell with glass windows coupled to a microscope (Axiotech 100 HD reflected-light microscope, Zeiss, Germany).[69]

Poke-flow measurements. The poke-flow technique was used to constrain the viscosities of the inner and outer phases of the BBOA particles.[70–72] Poke flow measurements were done on the same prepared samples used for the phase behaviour measurements. The setup was similar to that used previously.[71–74] The samples were put in a humidified flow cell which has a window on the bottom to allow viewing by an inverted microscope (ME1400TC-INF, AmScope, USA). The cell also has a hole in the top, sealed by a flexible latex membrane, through which an ultrafine needle (13561-10, Ted Pella Inc., USA) is inserted. The needle is moved using a micromanipulator to poke BBOA particles. Experiments were conducted at 30%, 40%, 50% and 60% RH, and the particles were conditioned in the flow cell for 3 hours before being poked. Poking caused the particles to crack if they were highly viscous, or else resulted in the formation of a hole in the particle which would recover over time to reduce the surface free energy of the system. Images of the particles were recorded for 2 hours after poking.

If an individual phase cracked and did not flow during the 2 hour observation time, the viscosity was assigned to $\gtrsim 2.5 \times 10^8$ Pa s based on fluid dynamics simulations with a quarter sphere model of a cracked particle.[71,73,74] This is based on the lowest viscosity that would be required for the cracked particle to move less than 0.5 µm in 2 hours, as any movement less than that would be undetectable on the microscope. If there was no cracking and rather a hole formed in an individual phase and slowly recovered over time we did not attempt to assign a viscosity. Fluid dynamics simulations based on a half torus model have been developed to determine the viscosity of single phase particles that formed a hole after poking and slowly recovered.[71,72] However, this approach does not precisely capture the physics for two phase particles, and hence was not applied here. Our approach of only assigning a viscosity to multiphase particles that cracked and did not flow is similar to the approach used by Song et al. to constrain the viscosity of field collected multiphase samples.[74,75]

Aerosol Mass Spectrometry. A high-resolution time-of-flight Aerosol Mass Spectrometer (HR-ToF-AMS) (Aerodyne, USA) was used to measure the mass spectra of the field and lab sample extracts. The working principle and operation of the HR-ToF-AMS are described in detail elsewhere;[77–79] briefly, the AMS measures electron-ionization mass spectra of aerosol particles sampled from ambient air and can report the bulk aerosol quantities of organics, nitrate, sulfate, ammonium and chloride mass concentrations. The vaporizer current was set to 1 A. To prepare the sample in a form that could be sampled by the AMS, extracts were nebulized using the same syringe pump pneumatic nebulizer used for the phase behaviour measurements (Figure S3). After nebulization, samples were diluted and dried with a sheath gas flow of 10 to 15 L min^{-1}. The aerosol then passed through a home-built diffusion dryer packed with 30 cm of molecular sieves (Type 4A beads 8-12 mesh, Supelco, Germany) and 30 cm of activated charcoal (Sigma-Aldrich,

USA) to remove any residual water and methanol, respectively, and then sampled by the AMS (Figure S3). High-resolution AMS data were processed using Squirrel v1.65F and PIKA 1.25F in the Igor Pro software environment (WaveMetrics, USA). Elemental ratios were estimated using the Improved Ambient method[80] using peaks up to m/z 180, since over 93% of the mass was contained in m/z below 180 for all samples. For each sample, we report the mean oxygen-to-carbon ratio (O:C), hydrogen-to-carbon ratio (H:C), and carbon oxidation state ($\overline{OS}_C, \approx 2 \times O:C - H:C$).[81]

Results and Discussion

Chemical composition of the BBOA particles. The AMS results (Table 1) indicate that both the field and lab BBOA samples were mainly organic (> 90 wt %), which is consistent with previous measurements of BBOA from laboratory burns of pine wood.[11] The AMS results also show that the field BBOA was more oxidized than the lab BBOA, with mean O:C values ranging from 0.73-0.75 for field samples compared to 0.56 for the lab generated BBOA (Table 1). The higher degree of oxidation of the field samples could be due to aging of primary BBOA in the atmosphere by ozone and OH radicals. During aging, primary BBOA (BBOA emitted directly to the atmosphere) also takes up secondary BBOA (BBOA formed in the atmosphere by the oxidation of volatile organic compounds in the smoke plumes) which would further increase the overall oxidation state of the BBOA.[58] Other factors expected to have contributed to the difference in O:C include more dilution of the field samples compared to the lab-generated smoke, allowing for the evaporation of lower O:C compounds, and differences in combustion conditions between the field and laboratory (e.g. flaming vs smoldering), which could have influenced the O:C of the BBOA in either direction.

Table 1. Composition and oxidation state of BBOA samples obtained from AMS analysis.

Sample	Mass fraction					Mean oxidation		
	Organic	NO$_3$	NH$_4$	SO$_4$	Cl	O:C	H:C	$\overline{OS}$c
Kamloops	0.93	0.032	0.026	0.0075	0.0055	0.73 ± 0.20^a	1.44 ± 0.19^b	0.02 ± 0.5^c
Kelowna	0.94	0.024	0.035	0.0041	0.0023	0.75 ± 0.21	1.46 ± 0.14	0.04 ± 0.5
Lab	0.95	0.039	0.010	0.0023	0.00036	0.56 ± 0.16	1.69 ± 0.22	-0.57 ± 0.5

^{a,b} The uncertainties for O:C and H:C ratios are 28% and 13%, respectively, based on the results for standards reported by Canagaratna et al. for the improved ambient method.[80]

^{c} The ± 0.5 uncertainty associated with $\overline{OS}$c is also from the improved ambient method.[80]
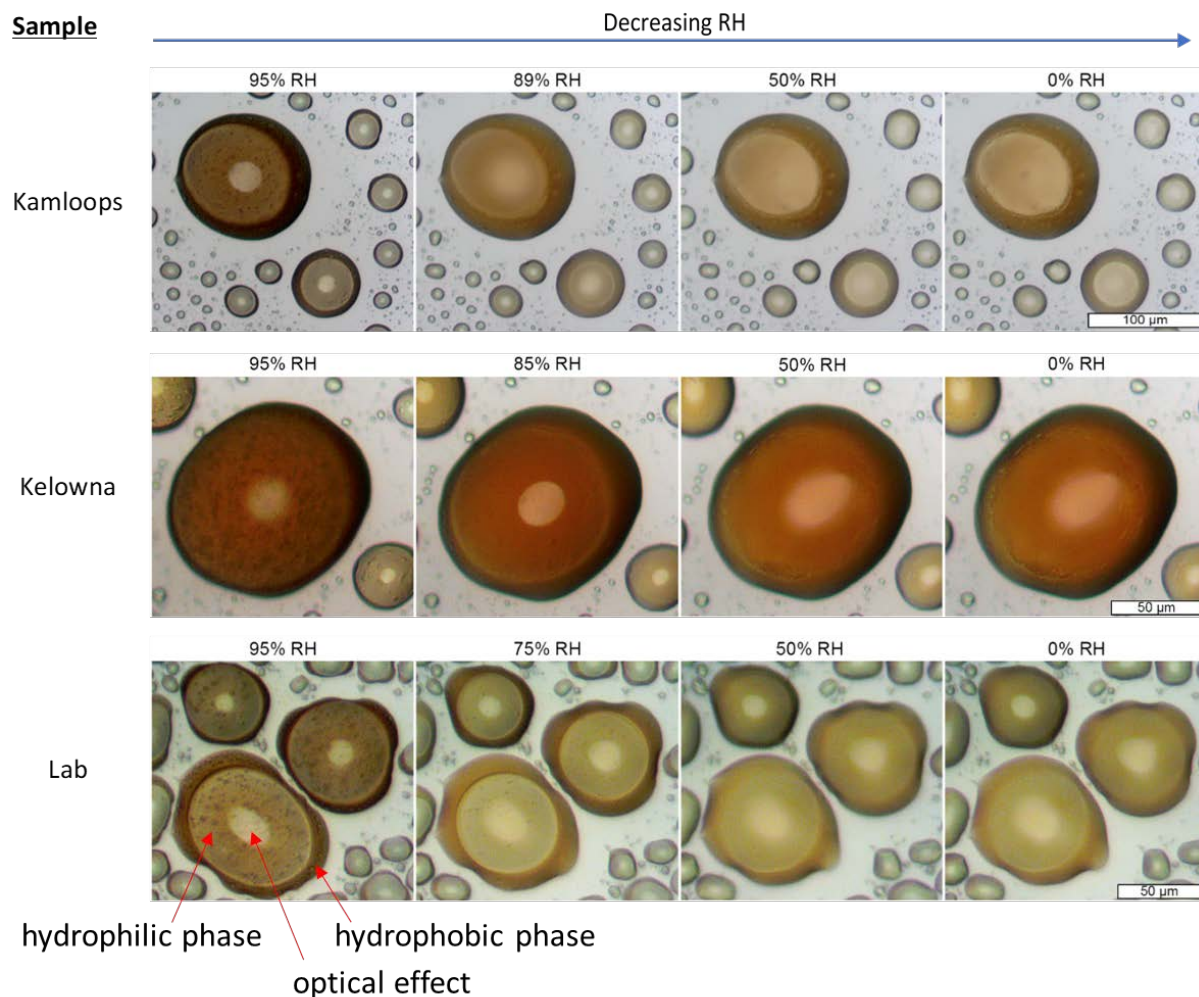
Figure 1. Images from the Kamloops field sample (top), Kelowna field sample (middle), and laboratory-generated BBOA (bottom) extracts, showing two phases, as the RH was decreased from ~95% to 0%. The images and RH values in the figure were selected to show a representative range of the BBOA's phase behavior. The small white ellipses in the centers of many of the droplets are reflections/optical effects from the microscope's lamp.

Phase behavior. The lab generated BBOA samples, which were not aged and came only from pine wood, had two phases across the full range of RH values investigated (~95 – 0 % RH) (Figure 1). This observation is consistent with the results by Gregson et al. who also observed two phases in BBOA particles generated from smoldering pine wood using a generation system identical to that used here.[34] Gregson et al. sampled BBOA on slides without extracting with solvents. The good agreement between our results and the results from Gregson et al. suggests that most of the BBOA was extracted with the water-methanol mixture used in our experiments. Others have shown that phase separation can occur in mixtures of primary and secondary organic aerosols and mixtures of different types of secondary organic aerosols if the organic molecules making up the mixtures have a difference of > 0.2 in O:C values.[52,53,56,57] In addition, previous studies have shown that unaged BBOA can contain organic molecules with a wide range of O:C values.[2,81] Therefore,

phase separation in unaged lab BBOA can be explained by the large difference in O:C values of the organic molecules making up the BBOA.

Field sample extracts also showed multiple phases across the full range of RH values (Figure 1). These results can also likely be explained by a wide range of O:C values within primary BBOA created by the combustion and pyrolysis of cellulose and lignin. The field BBOA also likely contains secondary BBOA in addition to primary BBOA. Secondary BBOA should have organic molecules with higher O:C values than primary BBOA,[58,59] further enhancing phase separation when mixed with primary BBOA. Multiple phases in aerosols particles can also be driven by the coexistence of organic and inorganic salts which are soluble in water,[44,83−85] but the AMS results (Table 1) indicate that both the field and lab BBOA samples were mainly organic. Hence, the presence of inorganic salts was most likely not the main driver for multiple phases in the lab and field BBOA.

In most cases, the particles assumed an approximately core-shell morphology. The outer phase can be identified as a less polar, hydrophobic organic phase while the inner phase is the more polar and hydrophilic of the two. As humidity increased in the flow cell, the inner phase usually swelled, showing that it was more hydrophilic and more polar. Higher polarity is generally expected to lead to higher surface tension, thus the higher polarity compounds are expected to comprise the inner phase to minimize surface area, assuming enough time for diffusion and equilibration within the particles.[86] Others have shown that methanol-soluble BrC from biomass burning has a higher absorption of light than water-soluble BrC, suggesting that most of the colour comes from the less polar molecules.[87] We should therefore expect the low-polarity hydrophobic outer phase to be darker in colour, which is indeed observed in the particles in Figure 1.

Viscosity. The viscosities of the field and lab samples were probed using the poke-flow technique. If the particles cracked upon being poked and then did not show any signs of recovery after 2 hours, they were classified as being amorphous solid or semi-solid with viscosities of at least 2.5×10^8 Pa s.[71,73,74] Amorphous solids have a viscosity of $>10^{12}$ Pa s and semi-solids have a viscosity between 10^2 and 10^{12} Pa s.[88]

As shown in Figure 2 (top four rows), the Kamloops and Kelowna samples shattered at 30% RH and the shards did not show any signs of flowing. At 40% RH, the particles also shattered with no signs of flow. For the Kamloops sample, the poke in the center of the droplet did not cause cracks to extend all the way to the outer phase, so another poke was made in the outer phase as quickly as possible (near the top of the particle in Figure 2, second row), and this poke caused clear cracks in the outer phase. At 50% RH, poking the center of the Kamloops sample caused cracks in the outer phase but only a hole in the inner phase, without cracks. For the Kelowna sample at the same relative humidity, a poke in the center caused cracks from the center to the outer edge. Again, there were no signs of recovery in any of the cracked particles at 40 or 50% RH. We conclude that the field samples had at least one phase that was semi-solid or amorphous solid with a viscosity 2.5×10^8 Pa s for RH values of 50% or less.
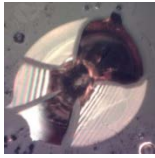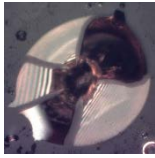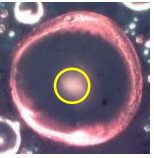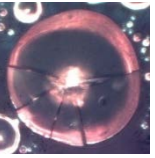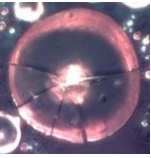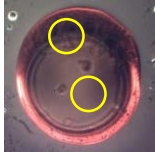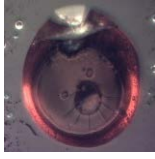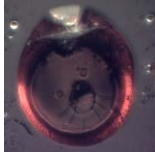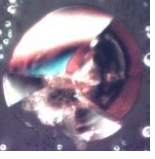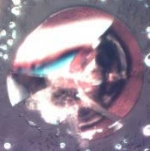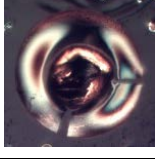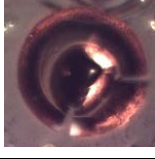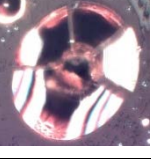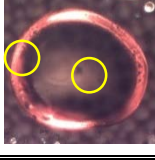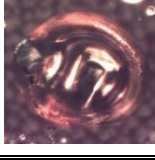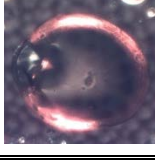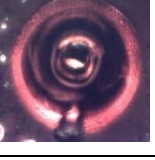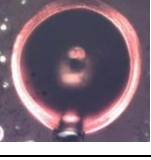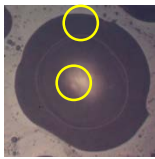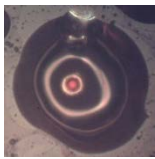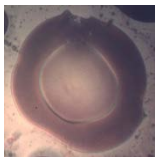
	Kamloops			Kelowna		
RH (%)	Before poking	Immediately after poking	2 hours	Before poking	Immediately after poking	2 hours
30						
40						
50						
60						

	Lab		
RH (%)	Before poking	Immediately after poking	2 hours
30			

Figure 2: Poke-flow results for the BBOA extracts at select RH values. Images were captured before the particles were poked, immediately after being poked, and then 2 hours after being poked. Yellow circles on the pre-poke images indicate where the particles were poked. The coloration of the droplets here looks different from those in Figure 1 because the microscope and the humidity-controlled cell are different, leading to different lighting.

At 60% RH, both field samples were poked once in the inner phase and once on the outer phase (Figure 2, fourth row), forming holes in the particles with no signs of cracking. After 2 hours, the hole in the middle almost fully recovered while the outer phase did not move. The unmoving outer phase may have been due to a difference in the surface tension at the outer edge of the droplet

compared to the middle and the thinness of the outer phase, or, alternatively, the outer phase may have been more viscous than the inner phase. Without fluid dynamics simulations, it is not possible to distinguish between these two cases.

Poking the lab generated sample at 30% RH resulted in a hole in the center of the particle that closed within one minute, showing a much lower viscosity than the field samples that cracked under the same conditions. The outer phase was also poked, and the hole recovered partially. When compared to the cracking and complete lack of flow in both the inner and outer phase of the field BBOA under the same 30% RH conditions, this shows that the lab samples are less viscous than field samples.

The difference in the viscosities of the lab and field samples can be explained, at least in part, by the higher oxidation of the field samples (Table 1), which should be expected to lead to more polar compounds, higher intermolecular forces, and therefore higher viscosities in the BBOA.[81,88,89] The differences in viscosities between the lab and field samples could also be due to the field samples having a greater degree of dilution in the atmosphere prior to sampling, which would result in low viscosity semivolatile organic compounds evaporating from the BBOA. The differences in viscosities could also be due to differences in burn conditions (i.e. flaming vs smoldering). Additional studies are needed to explore the effect of atmospheric oxidation, dilution, and burning conditions on BBOA viscosity.

Comparison with previous studies. As shown in Figure 3, the BBOA field samples have higher viscosities under more humid conditions than other BBOA samples that have been examined.[34,37,42,90] Kiland et al. used poke-flow to measure the viscosity of secondary organic aerosol made from the oxidation of BBOA-like phenolic compounds, as a proxy for biomass burning secondary organic aerosol. Those samples were highly viscous and cracked at low RH, but their viscosities decreased by an order of magnitude by 20% RH, and at 40% RH the droplets recovered too quickly to analyze with poke-flow which indicates a low viscosity, < 3000 Pa s.[42]

Schnitzler et al. used poke-flow to measure the viscosity of water-soluble extracts of primary BBOA generated in the lab from smoldering pine wood. At low RH, the water-soluble BBOA had a somewhat higher viscosity than the whole primary BBOA measured by Gregson et al.[34] This could be because only the more polar water-soluble molecules were extracted or because the methods to measure viscosity were different. The water-soluble BBOA consistently had a viscosity lower than Kiland et al.'s aerosols, and far lower than the field samples herein.[37] This points to an increase in BBOA viscosity caused by aging, oxidation, and the formation of SOA.

Gregson et al. used the fluorescence recovery after photobleaching (FRAP) method to measure the diffusion coefficients of fluorescent dyes in BBOA, and then converted the results into the viscosity of the hydrophobic phase and the hydrophilic phase of the BBOA. Gregson et al. reported viscosities of about 10^2 Pa s at 30% RH and 293 K for both phases, estimated from the diffusion coefficients measurements.[34] This is far lower than the field BBOA, but consistent with our findings that unaged laboratory generated BBOA recovered too quickly for the poke-flow method to measure.

Xu et al. reported the glass transition temperature and viscosity of unaged and aged BBOA generated from the combustion of pine wood using flaming conditions.[42] Glass transition temperatures and viscosities were calculated from volatility measurements, which assumes that the BBOA particles contained a single phase. At 35% RH and 298.15 K, they reported that the viscosity of pine BBOA was 2.5× higher after an OH exposure equivalent to 1.5 days in the atmosphere (Table S7 in Xu et al.), which is still approximately 3 orders of magnitude less viscous than our field BBOA samples at 30-40% RH.
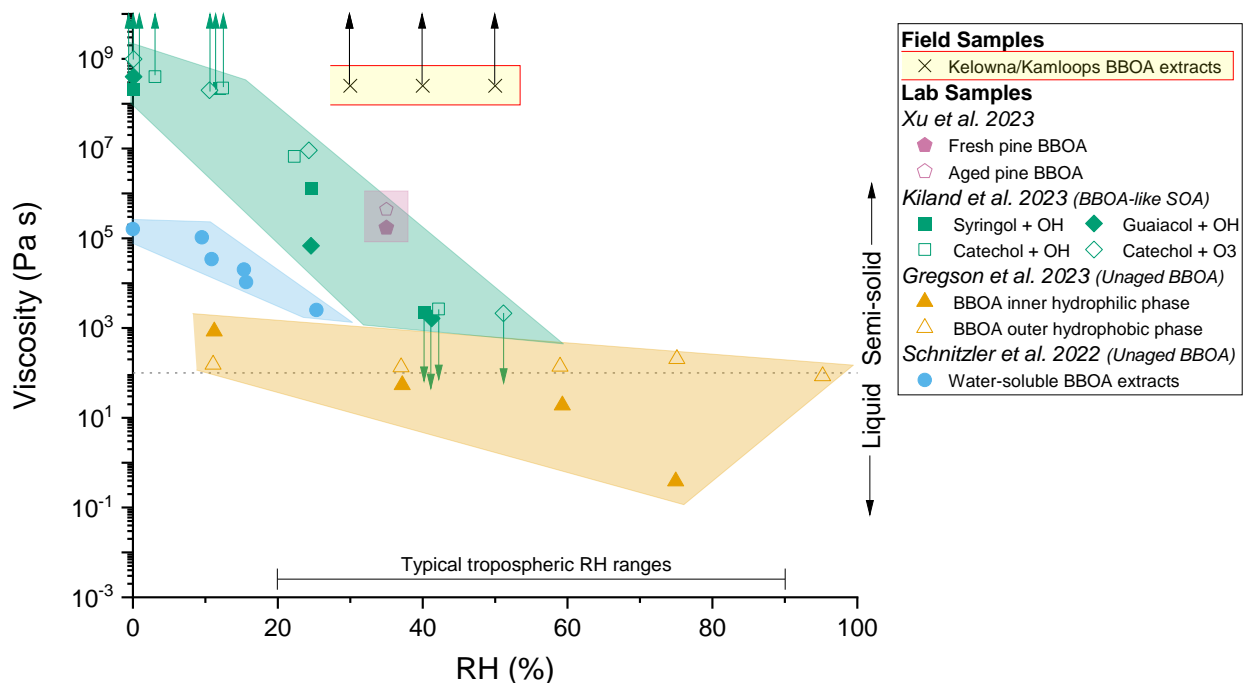
Figure 3. Previously measured viscosities of lab-generated primary pine BBOA (Schnitzler et al. 2022, Xu et al. 2023, and Gregson et al. 2023), oxidation flow reactor-aged pine BBOA (Xu et al. 2023), and oxidatively aged secondary BBOA proxies (Kiland et al. 2023) compared to the viscosities observed for the Kamloops and Kelowna field samples (the results from both field sites were the same and have been combined).[42,37,34] Upward and downward arrows on data points indicate that viscosities are a minimum or maximum value, respectively, for the viscosity of the aerosol under those conditions. The viscosity of the lab-generated BBOA in this study is assumed to be the same as the viscosities reported in Gregson et al. because the aerosol was generated from the same fuel and with the same conditions and equipment. The bar at the bottom shows the approximate range of relative humidity commonly found in the troposphere.[71,91,92]

Implications

Current atmospheric models that treat biomass burning organic aerosols typically consider them as single-phased particles.[37,47–49] The results herein show that BBOA, at least in regions where forests primarily consist of pine trees, should be treated as having two separate phases. Depending on the degree of internal/external mixing of organic aerosol in forest fire plumes, these two phases may coexist and be separated within individual particles. This is without considering the mixing state of soot/black carbon (BC) with BBOA in wildfire plumes, which can also have different degrees of internal and external mixing and depends on the age of the plume.[21,93,94] BC is often seen coated with a layer of BBOA, so if the BBOA is phase-separated, it is possible to have BC cores engulfed in 2 distinct layers of BBOA. In addition, BC in two-phased particles can preferentially partition into the lowest polarity phase depending on coating thickness, which may modify the absorption of sunlight by BC.[95,96]

Phase separation in aerosols impacts partitioning of species between the gas and particle phase. If BBOA contain a single phase, then semivolatile organic compounds can partition in to the entire aerosol mass. On the other hand, if phase separation occurs, semivolatile organic compounds may only partition into a portion of the aerosol mass, reducing the gas-to-particle partitioning of semivolatile organic compounds. Therefore, models that assume single-phase BBOA may be overestimating particle growth.[54,97–101] Phase separation can increase the cloud condensation nucleation activity of organic aerosols by moving the lower surface tension organics to the outside of the particle, so models on clouds and weather could also be misrepresenting the effects of biomass burning.[32,84]

In Schnitzler et al. and in Gregson et al., the viscosity of lab-generated BBOA was used to estimate the lifetime of BrC due to ozonolysis.[34,37] As BrC reacts with ozone, it can be "bleached" and lose its absorptive properties, changing its impact on the climate.[37,102] This process is slowed down when BBOA/BrC is highly viscous, as it takes longer for ozone to diffuse in to the aerosol. The experiments here predict that BBOA will be more viscous than previously reported, as the field BBOA was more viscous at higher RHs than both aqueous extracts and non-extracted lab-generated BBOA that have been studied before (Figure 3).[34,37] Under conditions where fresh lab-generated BBOA would be a liquid, the field sample BBOA would be a solid, and the lifetimes of processes like ozonolysis would be even longer. This framework can be extended and applied to other reactions in BBOA that have diffusion-limited kinetics.

Biomass burning events emit large amounts of primary BBOA and precursors of secondary BBOA. After emission the primary BBOA can partially evaporate and secondary BBOA can form on and in the primary BBOA.[48,58] A highly viscous BBOA, as observed here, could limit the rate of evaporation of primary BBOA and the formation rate of secondary BBOA.[103–108] A recent modelling study that investigated the evolution of BBOA by evaporation of primary BBOA and the formation of secondary BBOA assumed the BBOA was liquid-like with a diffusion coefficient of 10^{-10} m^2 s^{-1}.[48] Additional modelling studies are needed to determine the effect of highly viscous BBOA on the evolution of BBOA in the atmosphere and the resulting impact on predicted BBOA mass and composition.

The high viscosity may also have an impact on ice-cloud nucleation. Some studies have suggested that glassy organic aerosol can act as heterogeneous nuclei for ice clouds.[26,109–113] The forest fire BBOA in this study was only highly viscous up to 50% RH at room temperature, but viscosity also increases as temperatures get colder. Hence, the RH threshold at which cracking occurs will be extended to higher RH values at higher, colder altitudes. In the upper troposphere, where temperatures and RH values are often low,[91] BBOA might often be in an amorphous solid (i.e. glassy) state. Consistent with this speculation, previous studies have observed ice nucleation in smoke plumes in the free troposphere.[114] However, the nucleation of ice by glassy organic aerosol is still an active area of debate with a recent study suggesting that ice nucleation by glassy organic aerosol may be less important than previously suggested.[115] Ice nucleation by wildfire smoke can also be triggered by soot produced during flaming conditions or inorganic components and minerals present in biomass, and these mechanisms may explain the observations of ice nucleation in smoke plumes in the free troposphere.[116,117] Studies that focus on ice nucleation by glassy BBOA are needed to resolve the importance of glassy BBOA for ice cloud formation in the upper troposphere.

A caveat to the implications above is that the particles used in our work were 60 to 120 µm in diameter, which is at least several times larger than atmospheric particles (approximately 10 nm to 10 µm in diameter). Finite size effects can suppress liquid-liquid phase separation when the diameter is ≲ 40 nm.[118] In addition, finite size effects may sharply decrease viscosities of organic aerosols when the diameter is ≲ 100 nm.[119] Thus, we anticipate that our results apply to particles larger than approximately 100 nm, which covers most of the mass of BBOA in the atmosphere,[120–122] but experiments are needed to verify this hypothesis.

While both the lab-generated and field BBOA samples showed two phases, the viscosity of the field samples was notably higher. The viscosity of the field samples was also higher than that of previously measured lab-generated BBOA and BBOA proxies.[34,37,42] The field samples were more oxidized than the lab samples, as shown in the AMS experiments. Therefore, any BBOA studies using lab-generated aerosols as proxies for wildfire BBOA should be mindful of these differences. It is, however, useful to be able to make samples in the lab rather than collecting them in the field as it enables more extensive studies of BBOA behaviour. Experiments with aging and dilution should be done to bridge the gap between lab and field BBOA and to develop methods for creating more realistic BBOA in the laboratory environment.

Supporting Information

Additional figures: maps showing the locations of satellite-detected forest fires and calculated air back-trajectories during field sampling, air quality station data, and a schematic of the experimental setup.

Acknowledgements

References

(1) Chen, J.; Li, C.; Ristovski, Z.; Milic, A.; Gu, Y.; Islam, M. S.; Wang, S.; Hao, J.; Zhang, H.; He, C.; Guo, H.; Fu, H.; Miljevic, B.; Morawska, L.; Thai, P.; Lam, Y. F.; Pereira, G.; Ding, A.; Huang, X.; Dumka, U. C. A Review of Biomass Burning: Emissions and Impacts on Air Quality, Health and Climate in China. *Sci. Total Environ.* **2017**, *579* (November 2016), 1000–1034. https://doi.org/10.1016/j.scitotenv.2016.11.025.

(2) Zhou, S.; Collier, S.; Jaffe, D. A.; Briggs, N. L.; Hee, J.; Sedlacek III, A. J.; Kleinman, L.; Onasch, T. B.; Zhang, Q. Regional Influence of Wildfires on Aerosol Chemistry in the Western US and Insights into Atmospheric Aging of Biomass Burning Organic Aerosol. *Atmospheric Chem. Phys.* **2017**, *17* (3), 2477–2493. https://doi.org/10.5194/acp-17-2477-2017.

(3) Li, H.; Zhang, Q.; Jiang, W.; Collier, S.; Sun, Y.; Zhang, Q.; He, K. Characteristics and Sources of Water-Soluble Organic Aerosol in a Heavily Polluted Environment in Northern China. *Sci. Total Environ.* **2021**, *758*, 143970. https://doi.org/10.1016/j.scitotenv.2020.143970.

(4) Bozzetti, C.; Sosedova, Y.; Xiao, M.; Daellenbach, K. R.; Ulevicius, V.; Dudoitis, V.; Mordas, G.; Byčenkienė, S.; Plauškaitė, K.; Vlachou, A.; Golly, B.; Chazeau, B.; Besombes, J.-L.; Baltensperger, U.; Jaffrezo, J.-L.; Slowik, J. G.; El Haddad, I.; Prévôt, A. S. H. Argon Offline-AMS Source Apportionment of Organic Aerosol over Yearly Cycles for an Urban, Rural, and Marine Site in Northern Europe. *Atmospheric Chem. Phys.* **2017**, *17* (1), 117–141. https://doi.org/10.5194/acp-17-117-2017.

(5) Johnson, M. S.; Strawbridge, K.; Knowland, K. E.; Keller, C.; Travis, M. Long-Range Transport of Siberian Biomass Burning Emissions to North America during FIREX-AQ.

Atmos. Environ. **2021**, *252* (October 2020), 118241–118241. https://doi.org/10.1016/j.atmosenv.2021.118241.

(6)   Wu, Y.; Nehrir, A. R.; Ren, X.; Dickerson, R. R.; Huang, J.; Stratton, P. R.; Gronoff, G.; Kooi, S. A.; Collins, J. E.; Berkoff, T. A.; Lei, L.; Gross, B.; Moshary, F. Synergistic Aircraft and Ground Observations of Transported Wildfire Smoke and Its Impact on Air Quality in New York City during the Summer 2018 LISTOS Campaign. *Sci. Total Environ.* **2021**, *773*, 145030–145030. https://doi.org/10.1016/j.scitotenv.2021.145030.

(7)   Carter, T. S.; Heald, C. L.; Cappa, C. D.; Kroll, J. H.; Campos, T. L.; Coe, H.; Cotterell, M. I.; Davies, N. W.; Farmer, D. K.; Fox, C.; Garofalo, L. A.; Hu, L.; Langridge, J. M.; Levin, E. J. T.; Murphy, S. M.; Pokhrel, R. P.; Shen, Y.; Szpek, K.; Taylor, J. W.; Wu, H. Investigating Carbonaceous Aerosol and Its Absorption Properties From Fires in the Western United States (WE-CAN) and Southern Africa (ORACLES and CLARIFY). *J. Geophys. Res. Atmospheres* **2021**, *126* (15), 1–28. https://doi.org/10.1029/2021jd034984.

(8)   Schill, G. P.; Froyd, K. D.; Bian, H.; Kupc, A.; Williamson, C.; Brock, C. A.; Ray, E.; Hornbrook, R. S.; Hills, A. J.; Apel, E. C.; Chin, M.; Colarco, P. R.; Murphy, D. M. Widespread Biomass Burning Smoke throughout the Remote Troposphere. *Nat. Geosci.* **2020**, *13* (6), 422–427. https://doi.org/10.1038/s41561-020-0586-1.

(9)   Reid, J. S.; Eck, T. F.; Christopher, S. A.; Koppman, R.; Dubovik, O.; Eleuterio, D. P.; Holben, B. N.; Reid, E. A.; Zhang, J. A Review of Biomass Burning Emissions Part II: Intensive Physical Properties of Biomass Burning Particles. *Atmospheric Chem. Phys.* **2005**, *5*, 799–825. https://doi.org/10.5194/acp-5-799-2005.

(10)   Liu, X.; Huey, L. G.; Yokelson, R. J.; Selimovic, V.; Simpson, I. J.; Müller, M.; Jimenez, J. L.; Campuzano-Jost, P.; Beyersdorf, A. J.; Blake, D. R.; Butterfield, Z.; Choi, Y.; Crounse, J. D.; Day, D. A.; Diskin, G. S.; Dubey, M. K.; Fortner, E.; Hanisco, T. F.; Hu, W.; King, L. E.; Kleinman, L.; Meinardi, S.; Mikoviny, T.; Onasch, T. B.; Palm, B. B.; Peischl, J.; Pollack, I. B.; Ryerson, T. B.; Sachse, G. W.; Sedlacek, A. J.; Shilling, J. E.; Springston, S.; St. Clair, J. M.; Tanner, D. J.; Teng, A. P.; Wennberg, P. O.; Wisthaler, A.; Wolfe, G. M. Airborne Measurements of Western U.S. Wildfire Emissions: Comparison with Prescribed Burning and Air Quality Implications. *J. Geophys. Res. Atmospheres* **2017**, *122* (11), 6108–6129. https://doi.org/10.1002/2016jd026315.

(11)   May, A. A.; McMeeking, G. R.; Lee, T.; Taylor, J. W.; Craven, J. S.; Burling, I.; Sullivan, A. P.; Akagi, S.; Collett, J. L.; Flynn, M.; Coe, H.; Urbanski, S. P.; Seinfeld, J. H.; Yokelson, R. J.; Kreidenweis, S. M. Aerosol Emissions from Prescribed Fires in the United States: A Synthesis of Laboratory and Aircraft Measurements. *J. Geophys. Res. Atmospheres* **2014**, *119* (20), 11,826-11,849. https://doi.org/10.1002/2014jd021848.

(12)   Liu, Y.; Stanturf, J.; Goodrick, S. Trends in Global Wildfire Potential in a Changing Climate. *For. Ecol. Manag.* **2010**, *259* (4), 685–697. https://doi.org/10.1016/j.foreco.2009.09.002.

(13)   Liu, Y.; L. Goodrick, S.; A. Stanturf, J. Future U.S. Wildfire Potential Trends Projected Using a Dynamically Downscaled Climate Change Scenario. *For. Ecol. Manag.* **2013**, *294*, 120–135. https://doi.org/10.1016/j.foreco.2012.06.049.

(14)   de Groot, W. J.; Flannigan, M. D.; Cantin, A. S. Climate Change Impacts on Future Boreal Fire Regimes. *For. Ecol. Manag.* **2013**, *294*, 35–44. https://doi.org/10.1016/j.foreco.2012.09.027.

(15)   Abram, N. J.; Henley, B. J.; Sen Gupta, A.; Lippmann, T. J. R.; Clarke, H.; Dowdy, A. J.; Sharples, J. J.; Nolan, R. H.; Zhang, T.; Wooster, M. J.; Wurtzel, J. B.; Meissner, K. J.;

Pitman, A. J.; Ukkola, A. M.; Murphy, B. P.; Tapper, N. J.; Boer, M. M. Connections of Climate Change and Variability to Large and Extreme Forest Fires in Southeast Australia. *Commun. Earth Environ.* **2021**, *2* (1), 8. https://doi.org/10.1038/s43247-020-00065-8.

(16) Kim, Y. H.; Warren, S. H.; Krantz, Q. T.; King, C.; Jaskot, R.; Preston, W. T.; George, B. J.; Hays, M. D.; Landis, M. S.; Higuchi, M.; Demarini, D. M.; Gilmour, M. I. Mutagenicity and Lung Toxicity of Smoldering vs. Flaming Emissions from Various Biomass Fuels: Implications for Health Effects from Wildland Fires. *Environ. Health Perspect.* **2018**, *126* (1). https://doi.org/10.1289/EHP2200.

(17) Korsiak, J.; Pinault, L.; Christidis, T.; Burnett, R. T.; Abrahamowicz, M.; Weichenthal, S. Long-Term Exposure to Wildfires and Cancer Incidence in Canada: A Population-Based Observational Cohort Study. *Lancet Planet. Health* **2022**, *6* (5), e400–e409. https://doi.org/10.1016/S2542-5196(22)00067-5.

(18) Wang, S.; Gallimore, P. J.; Liu-Kang, C.; Yeung, K.; Campbell, S. J.; Utinger, B.; Liu, T.; Peng, H.; Kalberer, M.; Chan, A. W. H.; Abbatt, J. P. D. Dynamic Wood Smoke Aerosol Toxicity during Oxidative Atmospheric Aging. *Environ. Sci. Technol.* **2023**, *57* (3), 1246–1256. https://doi.org/10.1021/acs.est.2c05929.

(19) Pardo, M.; Li, C.; He, Q.; Levin-Zaidman, S.; Tsoory, M.; Yu, Q.; Wang, X.; Rudich, Y. Mechanisms of Lung Toxicity Induced by Biomass Burning Aerosols. *Part. Fibre Toxicol.* **2020**, *17*, 4. https://doi.org/10.1186/s12989-020-0337-x.

(20) Zhang, Y.; Forrister, H.; Liu, J.; DIbb, J.; Anderson, B.; Schwarz, J. P.; Perring, A. E.; Jimenez, J. L.; Campuzano-Jost, P.; Wang, Y.; Nenes, A.; Weber, R. J. Top-of-Atmosphere Radiative Forcing Affected by Brown Carbon in the Upper Troposphere. *Nat. Geosci.* **2017**, *10* (7), 486–489. https://doi.org/10.1038/ngeo2960.

(21) Brown, H.; Liu, X.; Pokhrel, R.; Murphy, S.; Lu, Z.; Saleh, R.; Mielonen, T.; Kokkola, H.; Bergman, T.; Myhre, G.; Skeie, R. B.; Watson-Paris, D.; Stier, P.; Johnson, B.; Bellouin, N.; Schulz, M.; Vakkari, V.; Beukes, J. P.; van Zyl, P. G.; Liu, S.; Chand, D. Biomass Burning Aerosols in Most Climate Models Are Too Absorbing. *Nat. Commun.* **2021**, *12* (1), 277–277. https://doi.org/10.1038/s41467-020-20482-9.

(22) Yue, S.; Zhu, J.; Chen, S.; Xie, Q.; Li, W.; Li, L.; Ren, H.; Su, S.; Li, P.; Ma, H.; Fan, Y.; Cheng, B.; Wu, L.; Deng, J.; Hu, W.; Ren, L.; Wei, L.; Zhao, W.; Tian, Y.; Pan, X.; Sun, Y.; Wang, Z.; Wu, F.; Liu, C.-Q.; Su, H.; Penner, J. E.; Pöschl, U.; Andreae, M. O.; Cheng, Y.; Fu, P. Brown Carbon from Biomass Burning Imposes Strong Circum-Arctic Warming. *One Earth* **2022**, *5* (3), 293–304. https://doi.org/10.1016/j.oneear.2022.02.006.

(23) Saleh, R. From Measurements to Models: Toward Accurate Representation of Brown Carbon in Climate Calculations. *Curr. Pollut. Rep.* **2020**, *6* (2), 90–104. https://doi.org/10.1007/s40726-020-00139-3.

(24) Chung, C. E.; Ramanathan, V.; Decremer, D. Observationally Constrained Estimates of Carbonaceous Aerosol Radiative Forcing. *Proc. Natl. Acad. Sci. U. S. A.* **2012**, *109* (29), 11624–11629. https://doi.org/10.1073/pnas.1203707109.

(25) Carrico, C. M.; Petters, M. D.; Kreidenweiss, S. M.; Collett, J. L.; Engling, G.; Malm, W. C. Aerosol Hygroscopicity and Cloud Droplet Activation of Extracts of Filters from Biomass Burning Experiments. *J. Geophys. Res. Atmospheres* **2008**, *113* (8). https://doi.org/10.1029/2007JD009274.

(26) Knopf, D. A.; Alpert, P. A.; Wang, B. The Role of Organic Aerosol in Atmospheric Ice Nucleation: A Review. *ACS Earth Space Chem.* **2018**, *2* (3), 168–202. https://doi.org/10.1021/acsearthspacechem.7b00120.

(27) Bougiatioti, A.; Bezantakos, S.; Stavroulas, I.; Kalivitis, N.; Kokkalis, P.; Biskos, G.; Mihalopoulos, N.; Papayannis, A.; Nenes, A. Biomass-Burning Impact on CCN Number, Hygroscopicity and Cloud Formation during Summertime in the Eastern Mediterranean. *Atmospheric Chem. Phys.* **2016**, *16* (11), 7389–7409. https://doi.org/10.5194/acp-16-7389-2016.

(28) Song, M.; Marcolli, C.; Krieger, U. K.; Zuend, A.; Peter, T. Liquid-Liquid Phase Separation in Aerosol Particles: Dependence on O:C, Organic Functionalities, and Compositional Complexity. *Geophys. Res. Lett.* **2012**, *39* (19), 1–5. https://doi.org/10.1029/2012GL052807.

(29) Zuend, A.; Marcolli, C.; Peter, T.; Seinfeld, J. H. Computation of Liquid-Liquid Equilibria and Phase Stabilities: Implications for RH-Dependent Gas/Particle Partitioning of Organic-Inorganic Aerosols. *Atmospheric Chem. Phys.* **2010**, *10* (16), 7795–7820. https://doi.org/10.5194/acp-10-7795-2010.

(30) Zuend, A.; Seinfeld, J. H. Modeling the Gas-Particle Partitioning of Secondary Organic Aerosol: The Importance of Liquid-Liquid Phase Separation. *Atmospheric Chem. Phys.* **2012**, *12* (9), 3857–3882. https://doi.org/10.5194/acp-12-3857-2012.

(31) Liu, P.; Song, M.; Zhao, T.; Gunthe, S. S.; Ham, S.; He, Y.; Qin, Y. M.; Gong, Z.; Amorim, J. C.; Bertram, A. K.; Martin, S. T. Resolving the Mechanisms of Hygroscopic Growth and Cloud Condensation Nuclei Activity for Organic Particulate Matter. *Nat. Commun.* **2018**, *9* (1), 4076. https://doi.org/10.1038/s41467-018-06622-2.

(32) Renbaum-Wolff, L.; Song, M.; Marcolli, C.; Zhang, Y.; Liu, P. F.; Grayson, J. W.; Geiger, F. M.; Martin, S. T.; Bertram, A. K. Observations and Implications of Liquid–Liquid Phase Separation at High Relative Humidities in Secondary Organic Material Produced by α-Pinene Ozonolysis without Inorganic Salts. *Atmospheric Chem. Phys.* **2016**, *16* (12), 7969–7979. https://doi.org/10.5194/acp-16-7969-2016.

(33) Ovadnevaite, J.; Zuend, A.; Laaksonen, A.; Sanchez, K. J.; Roberts, G.; Ceburnis, D.; Decesari, S.; Rinaldi, M.; Hodas, N.; Facchini, M. C.; Seinfeld, J. H.; C, O. D. Surface Tension Prevails over Solute Effect in Organic-Influenced Cloud Droplet Activation. *Nature* **2017**, *546* (7660), 637–641. https://doi.org/10.1038/nature22806.

(34) Gregson, F. K. A.; Gerrebos, N. G. A.; Schervish, M.; Nikkho, S.; Schnitzler, E. G.; Schwartz, C.; Carlsten, C.; Abbatt, J. P. D.; Kamal, S.; Shiraiwa, M.; Bertram, A. K. Phase Behavior and Viscosity in Biomass Burning Organic Aerosol and Climatic Impacts. *Environ. Sci. Technol.* **2023**, *57* (39), 14548–14557. https://doi.org/10.1021/acs.est.3c03231.

(35) Schmedding, R.; Ma, M. T.; Zhang, Y.; Farrell, S.; Pye, H. O. T.; Chen, Y. Z.; Wang, C. T.; Rasool, Q. Z.; Budisulistiorini, S. H.; Ault, A. P.; Surratt, J. D.; Vizuete, W. Alpha-Pinene-Derived Organic Coatings on Acidic Sulfate Aerosol Impacts Secondary Organic aerJosol Formation from Isoprene in a Box Model. *Atmos. Environ.* **2019**, *213*, 456–462. https://doi.org/10.1016/j.atmosenv.2019.06.005.

(36) Zhang, Y.; Chen, Y.; Lambe, A. T.; Olson, N. E.; Lei, Z.; Craig, R. L.; Zhang, Z.; Gold, A.; Onasch, T. B.; Jayne, J. T.; Worsnop, D. R.; Gaston, C. J.; Thornton, J. A.; Vizuete, W.; Ault, A. P.; Surratt, J. D. Effect of the Aerosol-Phase State on Secondary Organic Aerosol Formation from the Reactive Uptake of Isoprene-Derived Epoxydiols (IEPOX). *Environ. Sci. Technol. Lett.* **2018**, *5* (3), 167–174. https://doi.org/10.1021/acs.estlett.8b00044.

(37) Schnitzler, E. G.; Gerrebos, N. G. A.; Carter, T. S.; Huang, Y.; Heald, C. L.; Bertram, A. K.; Abbatt, J. P. D. Rate of Atmospheric Brown Carbon Whitening Governed by

Environmental Conditions. *Proc. Natl. Acad. Sci.* **2022**, *119* (38). https://doi.org/10.1073/pnas.2205610119.

(38) Rasool, Q. Z.; Shrivastava, M.; Liu, Y.; Gaudet, B.; Zhao, B. Modeling the Impact of the Organic Aerosol Phase State on Multiphase OH Reactive Uptake Kinetics and the Resultant Heterogeneous Oxidation Timescale of Organic Aerosol in the Amazon Rainforest. *ACS Earth Space Chem.* **2023**, *7* (5), 1009–1024. https://doi.org/10.1021/acsearthspacechem.2c00366.

(39) Schnitzler, E. G.; Abbatt, J. P. D. Heterogeneous OH Oxidation of Secondary Brown Carbon Aerosol. *Atmospheric Chem. Phys.* **2018**, *18* (19), 14539–14553. https://doi.org/10.5194/acp-18-14539-2018.

(40) Alpert, P. A.; Arroyo, P. C.; Dou, J.; Krieger, U. K.; Steimer, S. S.; Förster, J.-D.; Ditas, F.; Pöhlker, C.; Rossignol, S.; Passananti, M.; Perrier, S.; George, C.; Shiraiwa, M.; Berkemeier, T.; Watts, B.; Ammann, M. Visualizing Reaction and Diffusion in Xanthan Gum Aerosol Particles Exposed to Ozone. *Phys. Chem. Chem. Phys.* **2019**, *21* (37), 20613–20627. https://doi.org/10.1039/C9CP03731D.

(41) Li, J.; Forrester, S. M.; Knopf, D. A. Heterogeneous Oxidation of Amorphous Organic Aerosol Surrogates by O_3, NO_3, and OH at Typical Tropospheric Temperatures. *Atmospheric Chem. Phys.* **2020**, *20* (10), 6055–6080. https://doi.org/10.5194/acp-20-6055-2020.

(42) Xu, W.; Li, Z.; Zhang, Z.; Li, J.; Karnezi, E.; Lambe, A. T.; Zhou, W.; Sun, J.; Du, A.; Li, Y.; Sun, Y. Changes in Physicochemical Properties of Organic Aerosol During Photochemical Aging of Cooking and Burning Emissions. *J. Geophys. Res. Atmospheres* **2023**, *128* (14), e2022JD037911. https://doi.org/10.1029/2022JD037911.

(43) Jahn, L. G.; Jahl, L. G.; Bowers, B. B.; Sullivan, R. C. Morphology of Organic Carbon Coatings on Biomass-Burning Particles and Their Role in Reactive Gas Uptake. *ACS Earth Space Chem.* **2021**, *5* (9), 2184–2195. https://doi.org/10.1021/acsearthspacechem.1c00237.

(44) Hettiyadura, A. P. S.; Garcia, V.; Li, C.; West, C. P.; Tomlin, J.; He, Q.; Rudich, Y.; Laskin, A. Chemical Composition and Molecular-Specific Optical Properties of Atmospheric Brown Carbon Associated with Biomass Burning. *Environ. Sci. Technol.* **2021**, *55* (4), 2511–2521. https://doi.org/10.1021/acs.est.0c05883.

(45) Li, C.; He, Q.; Schade, J.; Passig, J.; Zimmermann, R.; Meidan, D.; Laskin, A.; Rudich, Y. Dynamic Changes in Optical and Chemical Properties of Tar Ball Aerosols by Atmospheric Photochemical Aging. *Atmospheric Chem. Phys.* **2019**, *19* (1), 139–163. https://doi.org/10.5194/acp-19-139-2019.

(46) Zhuravleva, T. B.; Nasrtdinov, I. M.; Konovalov, I. B.; Golovushkin, N. A.; Beekmann, M. Impact of the Atmospheric Photochemical Evolution of the Organic Component of Biomass Burning Aerosol on Its Radiative Forcing Efficiency: A Box Model Analysis. *Atmosphere* **2021**, *12* (12), 1555. https://doi.org/10.3390/atmos12121555.

(47) Akherati, A.; He, Y.; Garofalo, L. A.; Hodshire, A. L.; Farmer, D. K.; Kreidenweis, S. M.; Permar, W.; Hu, L.; Fischer, E. V.; Jen, C. N.; Goldstein, A. H.; Levin, E. J. T.; DeMott, P. J.; Campos, T. L.; Flocke, F.; Reeves, J. M.; Toohey, D. W.; Pierce, J. R.; Jathar, S. H. Dilution and Photooxidation Driven Processes Explain the Evolution of Organic Aerosol in Wildfire Plumes. *Environ. Sci. Atmospheres* **2022**, *2* (5), 1000–1022. https://doi.org/10.1039/D1EA00082A.

(48) Patoulias, D.; Kallitsis, E.; Posner, L.; Pandis, S. N. Modeling Biomass Burning Organic Aerosol Atmospheric Evolution and Chemical Aging. *Atmosphere* **2021**, *12* (12), 1638. https://doi.org/10.3390/atmos12121638.

(49) Al-Mashala, H. H.; Betz, K. L.; Calvert, C. T.; Barton, J. A.; Bruce, E. E.; Schnitzler, E. G. Ultraviolet Irradiation Can Increase the Light Absorption and Viscosity of Primary Brown Carbon from Biomass Burning. *ACS Earth Space Chem.* **2023**, *7* (10), 1882–1889. https://doi.org/10.1021/acsearthspacechem.3c00155.

(50) Feng, T.; Wang, Y.; Hu, W.; Zhu, M.; Song, W.; Chen, W.; Sang, Y.; Fang, Z.; Deng, W.; Fang, H.; Yu, X.; Wu, C.; Yuan, B.; Huang, S.; Shao, M.; Huang, X.; He, L.; Lee, Y. R.; Huey, L. G.; Canonaco, F.; Prevot, A. S. H.; Wang, X. Impact of Aging on the Sources, Volatility, and Viscosity of Organic Aerosols in Chinese Outflows. *Atmospheric Chem. Phys.* **2023**, *23* (1), 611–636. https://doi.org/10.5194/acp-23-611-2023.

(51) Mahrt, F.; Newman, E.; Huang, Y.; Ammann, M.; Bertram, A. K. Phase Behavior of Hydrocarbon-like Primary Organic Aerosol and Secondary Organic Aerosol Proxies Based on Their Elemental Oxygen-to-Carbon Ratio. *Environ. Sci. Technol.* **2021**. https://doi.org/10.1021/acs.est.1c02697.

(52) Mahrt, F.; Peng, L.; Zaks, J.; Huang, Y.; Ohno, P. E.; Smith, N. R.; Gregson, F. K. A.; Qin, Y.; Faiola, C. L.; Martin, S. T.; Nizkorodov, S. A.; Ammann, M.; Bertram, A. K. Not All Types of Secondary Organic Aerosol Mix: Two Phases Observed When Mixing Different Secondary Organic Aerosol Types. *Atmospheric Chem. Phys.* **2022**, *22* (20), 13783–13796. https://doi.org/10.5194/acp-22-13783-2022.

(53) Song, M.; Marcolli, C.; Krieger, U. K.; Zuend, A.; Peter, T. Liquid-Liquid Phase Separation in Aerosol Particles: Dependence on O:C, Organic Functionalities, and Compositional Complexity. *Geophys. Res. Lett.* **2012**, *39* (19), 1–5. https://doi.org/10.1029/2012GL052807.

(54) Schmedding, R.; Rasool, Q. Z.; Zhang, Y.; Pye, H. O. T.; Zhang, H.; Chen, Y.; Surratt, J. D.; Lopez-Hilfiker, F. D.; Thornton, J. A.; Goldstein, A. H.; Vizuete, W. Predicting Secondary Organic Aerosol Phase State and Viscosity and Its Effect on Multiphase Chemistry in a Regional-Scale Air Quality Model. *Atmospheric Chem. Phys.* **2020**, *20* (13), 8201–8225. https://doi.org/10.5194/acp-20-8201-2020.

(55) Mahrt, F.; Huang, Y.; Zaks, J.; Devi, A.; Peng, L.; Ohno, P. E.; Qin, Y. M.; Martin, S. T.; Ammann, M.; Bertram, A. K. Phase Behavior of Internal Mixtures of Hydrocarbon-like Primary Organic Aerosol and Secondary Aerosol Based on Their Differences in Oxygen-to-Carbon Ratios. *Environ. Sci. Technol.* **2022**, *56* (7), 3960–3973. https://doi.org/10.1021/acs.est.1c07691.

(56) Gorkowski, K.; Donahue, N. M.; Sullivan, R. C. Aerosol Optical Tweezers Constrain the Morphology Evolution of Liquid-Liquid Phase-Separated Atmospheric Particles. *Chem* **2020**, *6* (1), 204–220. https://doi.org/10.1016/j.chempr.2019.10.018.

(57) Hodshire, A. L.; Akherati, A.; Alvarado, M. J.; Brown-Steiner, B.; Jathar, S. H.; Jimenez, J. L.; Kreidenweis, S. M.; Lonsdale, C. R.; Onasch, T. B.; Ortega, A. M.; Pierce, J. R. Aging Effects on Biomass Burning Aerosol Mass and Composition: A Critical Review of Field and Laboratory Studies. *Environ. Sci. Technol.* **2019**, *53* (17), 10007–10022. https://doi.org/10.1021/acs.est.9b02588.

(58) Ortega, A. M.; Day, D. A.; Cubison, M. J.; Brune, W. H.; Bon, D.; de Gouw, J. A.; Jimenez, J. L. Secondary Organic Aerosol Formation and Primary Organic Aerosol

Oxidation from Biomass-Burning Smoke in a Flow Reactor during FLAME-3. *Atmospheric Chem. Phys.* **2013**, *13* (22), 11551–11571. https://doi.org/10.5194/acp-13-11551-2013.

(59) British Columbia Ministry of Environment. *Envista - Air Resources Manager*. B.C. Air Data Archive. https://envistaweb.env.gov.bc.ca/ (accessed 2024-04-09).

(60) NASA. *FIRMS US/CANADA*. https://firms.modaps.eosdis.nasa.gov/map/ (accessed 2024-04-09).

(61) Wulder, M. A. *BC Tree Species Map/Likelihoods 2015 - Open Government Portal*. https://open.canada.ca/data/en/dataset/8dddaa7f-c60d-4802-a662-2930c5aeedb8 (accessed 2024-03-01).

(62) Hamann, A.; Smets, P.; Yanchuk, A. D.; Aitken, S. N. An Ecogeographic Framework for in Situ Conservation of Forest Trees in British Columbia. *Can. J. For. Res.* **2005**, *35* (11), 2553–2561. https://doi.org/10.1139/x05-181.

(63) Rolph, G.; Stein, A.; Stunder, B. Real-Time Environmental Applications and Display sYstem: READY. *Environ. Model. Softw.* **2017**, *95*, 210–228. https://doi.org/10.1016/j.envsoft.2017.06.025.

(64) NOAA Air Resources Laboratory. *READY - Real-time Environmental Applications and Display sYstem*. https://www.ready.noaa.gov/index.php (accessed 2024-04-09).

(65) Hems, R. F.; Schnitzler, E. G.; Bastawrous, M.; Soong, R.; Simpson, A. J.; Abbatt, J. P. D. Aqueous Photoreactions of Wood Smoke Brown Carbon. *ACS Earth Space Chem.* **2020**, *4* (7), 1149–1160. https://doi.org/10.1021/acsearthspacechem.0c00117.

(66) Trofimova, A.; Hems, R. F.; Liu, T.; Abbatt, J. P. D.; Schnitzler, E. G. Contribution of Charge-Transfer Complexes to Absorptivity of Primary Brown Carbon Aerosol. *ACS Earth Space Chem.* **2019**, *3* (8), 1393–1401. https://doi.org/10.1021/acsearthspacechem.9b00116.

(67) Greenspan, L. Humidity Fixed Points of Binary Saturated Aqueous Solutions. *J. Res. Natl. Bur. Stand. Sect. Phys. Chem.* **1977**, *81* (1), 89–96.

(68) Parsons, M. T.; Mak, J.; Lipetz, S. R.; Bertram, A. K. Deliquescence of Malonic, Succinic, Glutaric, and Adipic Acid Particles. *J. Geophys. Res. Atmospheres* **2004**, *109* (D6). https://doi.org/10.1029/2003JD004075.

(69) Murray, B. J.; Haddrell, A. E.; Peppe, S.; Davies, J. F.; Reid, J. P.; O'Sullivan, D.; Price, H. C.; Kumar, R.; Saunders, R. W.; Plane, J. M. C.; Umo, N. S.; Wilson, T. W. Glass Formation and Unusual Hygroscopic Growth of Iodic Acid Solution Droplets with Relevance for Iodine Mediated Particle Formation in the Marine Boundary Layer. *Atmospheric Chem. Phys.* **2012**, *12* (18), 8575–8587. https://doi.org/10.5194/acp-12-8575-2012.

(70) Renbaum-Wolff, L.; Grayson, J. W.; Bateman, A. P.; Kuwata, M.; Sellier, M.; Murray, B. J.; Shilling, J. E.; Martin, S. T.; Bertram, A. K. Viscosity of α-Pinene Secondary Organic Material and Implications for Particle Growth and Reactivity. *Proc. Natl. Acad. Sci. U. S. A.* **2013**, *110* (20), 8014–8019. https://doi.org/10.1073/pnas.1219548110.

(71) Grayson, J. W.; Song, M.; Sellier, M.; Bertram, A. K. Validation of the Poke-Flow Technique Combined with Simulations of Fluid Flow for Determining Viscosities in Samples with Small Volumes and High Viscosities. *Atmospheric Meas. Tech.* **2015**, *8* (6), 2463–2472. https://doi.org/10.5194/amt-8-2463-2015.

(72) Smith, N. R.; Crescenzo, G. V.; Bertram, A. K.; Nizkorodov, S. A.; Faiola, C. L. Insect Infestation Increases Viscosity of Biogenic Secondary Organic Aerosol. *ACS Earth Space Chem.* **2023**, *7* (5), 1060–1071. https://doi.org/10.1021/acsearthspacechem.3c00007.

(73) Smith, N. R.; Crescenzo, G. V.; Huang, Y.; Hettiyadura, A. P. S.; Siemens, K.; Li, Y.; Faiola, C. L.; Laskin, A.; Shiraiwa, M.; Bertram, A. K.; Nizkorodov, S. A. Viscosity and Liquid–Liquid Phase Separation in Healthy and Stressed Plant SOA. *Environ. Sci. Atmospheres* **2021**, *1* (3), 140–153. https://doi.org/10.1039/D0EA00020E.

(74) Song, M.; Jeong, R.; Kim, D.; Qiu, Y.; Meng, X.; Wu, Z.; Zuend, A.; Ha, Y.; Kim, C.; Kim, H.; Gaikwad, S.; Jang, K. S.; Lee, J. Y.; Ahn, J. Comparison of Phase States of PM(2.5) over Megacities, Seoul and Beijing, and Their Implications on Particle Size Distribution. *Env. Sci Technol* **2022**, *56* (24), 17581–17590. https://doi.org/10.1021/acs.est.2c06377.

(75) Gaikwad, S.; Jeong, R.; Kim, D.; Lee, K.; Jang, K.-S.; Kim, C.; Song, M. Microscopic Observation of a Liquid-Liquid-(Semi)Solid Phase in Polluted PM2.5. *Front. Environ. Sci.* **2022**, *10*.

(76) DeCarlo, P. F.; Kimmel, J. R.; Trimborn, A.; Northway, M. J.; Jayne, J. T.; Aiken, A. C.; Gonin, M.; Fuhrer, K.; Horvath, T.; Docherty, K. S.; Worsnop, D. R.; Jimenez, J. L. Field-Deployable, High-Resolution, Time-of-Flight Aerosol Mass Spectrometer. *Anal. Chem.* **2006**, *78* (24), 8281–8289. https://doi.org/10.1021/ac061249n.

(77) Aiken, A. C.; Decarlo, P. F.; Kroll, J. H.; Worsnop, D. R.; Huffman, J. A.; Docherty, K. S.; Ulbrich, I. M.; Mohr, C.; Kimmel, J. R.; Sueper, D.; Sun, Y.; Zhang, Q.; Trimborn, A.; Northway, M.; Ziemann, P. J.; Canagaratna, M. R.; Onasch, T. B.; Alfarra, M. R.; Prevot, A. S. H.; Dommen, J.; Duplissy, J.; Metzger, A.; Baltensperger, U.; Jimenez, J. L. O/C and OM/OC Ratios of Primary, Secondary, and Ambient Organic Aerosols with High-Resolution Time-of-Flight Aerosol Mass Spectrometry. *Environ. Sci. Technol.* **2008**, *42* (12), 4478--4485. https://doi.org/10.1021/es703009q.

(78) Aiken, A. C.; DeCarlo, P. F.; Jimenez, J. L. Elemental Analysis of Organic Species with Electron Ionization High-Resolution Mass Spectrometry. *Anal. Chem.* **2007**, *79* (21), 8350–8358. https://doi.org/10.1021/ac071150w.

(79) Canagaratna, M. R.; Jimenez, J. L.; Kroll, J. H.; Chen, Q.; Kessler, S. H.; Massoli, P.; Hildebrandt Ruiz, L.; Fortner, E.; Williams, L. R.; Wilson, K. R.; Surratt, J. D.; Donahue, N. M.; Jayne, J. T.; Worsnop, D. R. Elemental Ratio Measurements of Organic Compounds Using Aerosol Mass Spectrometry: Characterization, Improved Calibration, and Implications. *Atmospheric Chem. Phys.* **2015**, *15* (1), 253–272. https://doi.org/10.5194/acp-15-253-2015.

(80) Kroll, J. H.; Donahue, N. M.; Jimenez, J. L.; Kessler, S. H.; Canagaratna, M. R.; Wilson, K. R.; Altieri, K. E.; Mazzoleni, L. R.; Wozniak, A. S.; Bluhm, H.; Mysak, E. R.; Smith, J. D.; Kolb, C. E.; Worsnop, D. R. Carbon Oxidation State as a Metric for Describing the Chemistry of Atmospheric Organic Aerosol. *Nat. Chem.* **2011**, *3* (2), 133–139. https://doi.org/10.1038/nchem.948.

(81) DeRieux, W.-S. W.; Li, Y.; Lin, P.; Laskin, J.; Laskin, A.; Bertram, A. K.; Nizkorodov, S. A.; Shiraiwa, M. Predicting the Glass Transition Temperature and Viscosity of Secondary Organic Material Using Molecular Composition. *Atmospheric Chem. Phys.* **2018**, *18* (9), 6331–6351. https://doi.org/10.5194/acp-18-6331-2018.

(82) You, Y.; Smith, M. L.; Song, M.; Martin, S. T.; Bertram, A. K. Liquid–Liquid Phase Separation in Atmospherically Relevant Particles Consisting of Organic Species and Inorganic Salts. *Int. Rev. Phys. Chem.* **2014**, *33* (1), 43–77. https://doi.org/10.1080/0144235X.2014.890786.

(83) Freedman, M. A. Phase Separation in Organic Aerosol. *Chem. Soc. Rev.* **2017**, *46* (24), 7694–7705. https://doi.org/10.1039/c6cs00783j.

(84) Sun, H.; Biedermann, L.; Bond, T. C. Color of Brown Carbon: A Model for Ultraviolet and Visible Light Absorption by Organic Carbon Aerosol. *Geophys. Res. Lett.* **2007**, *34* (17). https://doi.org/10.1029/2007GL029797.

(85) Reid, J. P.; Dennis-Smither, B. J.; Kwamena, N.-O. A.; Miles, R. E. H.; Hanford, K. L.; Homer, C. J. The Morphology of Aerosol Particles Consisting of Hydrophobic and Hydrophilic Phases: Hydrocarbons, Alcohols and Fatty Acids as the Hydrophobic Component. *Phys. Chem. Chem. Phys.* **2011**, *13* (34), 15559–15572. https://doi.org/10.1039/C1CP21510H.

(86) Rana, A.; Dey, S.; Sarkar, S. Chapter 16 - Optical Properties of Brown Carbon in Aerosols and Surface Snow at Ny-Ålesund during the Polar Summer. In *Understanding Present and Past Arctic Environments*; Khare, N., Ed.; Elsevier, 2021; pp 343–356. https://doi.org/10.1016/B978-0-12-822869-2.00022-0.

(87) Mikhailov, E.; Vlasenko, S.; Martin, S. T.; Koop, T.; Pöschl, U. Amorphous and Crystalline Aerosol Particles Interacting with Water Vapor: Conceptual Framework and Experimental Evidence for Restructuring, Phase Transitions and Kinetic Limitations. *Atmospheric Chem. Phys.* **2009**, *9* (24), 9491–9522. https://doi.org/10.5194/acp-9-9491-2009.

(88) Grayson, J. W.; Evoy, E.; Song, M.; Chu, Y.; Maclean, A.; Nguyen, A.; Upshur, M. A.; Ebrahimi, M.; Chan, C. K.; Geiger, F. M.; Thomson, R. J.; Bertram, A. K. The Effect of Hydroxyl Functional Groups and Molar Mass on the Viscosity of Non-Crystalline Organic and Organic–Water Particles. *Atmospheric Chem. Phys.* **2017**, *17* (13), 8509–8524. https://doi.org/10.5194/acp-17-8509-2017.

(89) Rothfuss, N. E.; Petters, M. D. Characterization of the Temperature and Humidity-Dependent Phase Diagram of Amorphous Nanoscale Organic Aerosols. *Phys. Chem. Chem. Phys.* **2017**, *19* (9), 6532–6545. https://doi.org/10.1039/c6cp08593h.

(90) Kiland, K. J.; Mahrt, F.; Peng, L.; Nikkho, S.; Zaks, J.; Crescenzo, G. V.; Bertram, A. K. Viscosity, Glass Formation, and Mixing Times within Secondary Organic Aerosol from Biomass Burning Phenolics. *ACS Earth Space Chem.* **2023**, *7* (7), 1388–1400. https://doi.org/10.1021/acsearthspacechem.3c00039.

(91) Ruzmaikin, A.; Aumann, H. H.; Manning, E. M. Relative Humidity in the Troposphere with AIRS. *J. Atmospheric Sci.* **2014**, *71* (7), 2516–2533. https://doi.org/10.1175/JAS-D-13-0363.1.

(92) Lang, T.; Naumann, A. K.; Stevens, B.; Buehler, S. A. Tropical Free-Tropospheric Humidity Differences and Their Effect on the Clear-Sky Radiation Budget in Global Storm-Resolving Models. *J. Adv. Model. Earth Syst.* **2021**, *13* (11), e2021MS002514. https://doi.org/10.1029/2021MS002514.

(93) Sedlacek, A. J. I.; Lewis, E. R.; Onasch, T. B.; Zuidema, P.; Redemann, J.; Jaffe, D.; Kleinman, L. I. Using the Black Carbon Particle Mixing State to Characterize the Lifecycle of Biomass Burning Aerosols. *Environ. Sci. Technol.* **2022**, *56* (20), 14315–14325. https://doi.org/10.1021/acs.est.2c03851.

(94) Lack, D. A.; Langridge, J. M.; Bahreini, R.; Cappa, C. D.; Middlebrook, A. M.; Schwarz, J. P. Brown Carbon and Internal Mixing in Biomass Burning Particles. *Proc. Natl. Acad. Sci.* **2012**, *109* (37), 14802–14807. https://doi.org/10.1073/pnas.1206575109.

(95) Brunamonti, S.; Krieger, U. K.; Marcolli, C.; Peter, T. Redistribution of Black Carbon in Aerosol Particles Undergoing Liquid-Liquid Phase Separation. *Geophys. Res. Lett.* **2015**, *42* (7), 2532–2539. https://doi.org/10.1002/2014GL062908.

(96) Zhang, J.; Wang, Y. Y.; Teng, X. M.; Liu, L.; Xu, Y. S.; Ren, L. H.; Shi, Z. B.; Zhang, Y.; Jiang, J. K.; Liu, D. T.; Hu, M.; Shao, L. Y.; Chen, J. M.; Martin, S. T.; Zhang, X. Y.; Li, W. J. Liquid-Liquid Phase Separation Reduces Radiative Absorption by Aged Black Carbon Aerosols. *Commun. Earth Environ.* **2022**, *3* (1). https://doi.org/10.1038/s43247-022-00462-1.

(97) Zuend, A.; Marcolli, C.; Peter, T.; Seinfeld, J. H. Computation of Liquid-Liquid Equilibria and Phase Stabilities: Implications for RH-Dependent Gas/Particle Partitioning of Organic-Inorganic Aerosols. *Atmospheric Chem. Phys.* **2010**, *10* (16), 7795–7820. https://doi.org/10.5194/acp-10-7795-2010.

(98) Pye, H. O. T.; Zuend, A.; Fry, J. L.; Isaacman-VanWertz, G.; Capps, S. L.; Appel, K. W.; Foroutan, H.; Xu, L.; Ng, N. L.; Goldstein, A. H. Coupling of Organic and Inorganic Aerosol Systems and the Effect on Gas–Particle Partitioning in the Southeastern US. *Atmospheric Chem. Phys.* **2018**, *18* (1), 357–370. https://doi.org/10.5194/acp-18-357-2018.

(99) Pye, H. O. T.; Murphy, B. N.; Xu, L.; Ng, N. L.; Carlton, A. G.; Guo, H.; Weber, R.; Vasilakos, P.; Appel, K. W.; Budisulistiorini, S. H.; Surratt, J. D.; Nenes, A.; Hu, W.; Jimenez, J. L.; Isaacman-VanWertz, G.; Misztal, P. K.; Goldstein, A. H. On the Implications of Aerosol Liquid Water and Phase Separation for Organic Aerosol Mass. *Atmospheric Chem. Phys.* **2017**, *17* (1), 343–369. https://doi.org/10.5194/acp-17-343-2017.

(100) Ye, J.; Gordon, C. A.; Chan, A. W. H. Enhancement in Secondary Organic Aerosol Formation in the Presence of Preexisting Organic Particle. *Environ. Sci. Technol.* **2016**, *50* (7), 3572–3579. https://doi.org/10.1021/acs.est.5b05512.

(101) Ye, J.; Van Rooy, P.; Adam, C. H.; Jeong, C.-H.; Urch, B.; Cocker, D. R. I.; Evans, G. J.; Chan, A. W. H. Predicting Secondary Organic Aerosol Enhancement in the Presence of Atmospherically Relevant Organic Particles. *ACS Earth Space Chem.* **2018**, *2* (10), 1035–1046. https://doi.org/10.1021/acsearthspacechem.8b00093.

(102) Browne, E. C.; Zhang, X.; Franklin, J. P.; Ridley, K. J.; Kirchstetter, T. W.; Wilson, K. R.; Cappa, C. D.; Kroll, J. H. Effect of Heterogeneous Oxidative Aging on Light Absorption by Biomass Burning Organic Aerosol. *Aerosol Sci. Technol.* **2019**, *53* (6), 663–674. https://doi.org/10.1080/02786826.2019.1599321.

(103) Zelenyuk, A.; Imre, D.; Beránek, J.; Abramson, E.; Wilson, J.; Shrivastava, M. Synergy between Secondary Organic Aerosols and Long-Range Transport of Polycyclic Aromatic Hydrocarbons. *Environ. Sci. Technol.* **2012**, *46* (22), 12459–12466. https://doi.org/10.1021/es302743z.

(104) Kim, Y.; Sartelet, K.; Couvidat, F. Modeling the Effect of Non-Ideality, Dynamic Mass Transfer and Viscosity on SOA Formation in a 3-D Air Quality Model. *Atmospheric Chem. Phys.* **2019**, *19* (2), 1241–1261. https://doi.org/10.5194/acp-19-1241-2019.

(105) Zaveri, R. A.; Shilling, J. E.; Zelenyuk, A.; Liu, J.; Bell, D. M.; D'Ambro, E. L.; Gaston, C. J.; Thornton, J. A.; Laskin, A.; Lin, P.; Wilson, J.; Easter, R. C.; Wang, J.; Bertram, A. K.; Martin, S. T.; Seinfeld, J. H.; Worsnop, D. R. Growth Kinetics and Size Distribution Dynamics of Viscous Secondary Organic Aerosol. *Environ. Sci. Technol.* **2018**, *52* (3), 1191–1199. https://doi.org/10.1021/acs.est.7b04623.

(106)   Shiraiwa, M.; Seinfeld, J. H. Equilibration Timescale of Atmospheric Secondary Organic Aerosol Partitioning. *Geophys. Res. Lett.* **2012**, *39* (24). https://doi.org/10.1029/2012GL054008.

(107)   Yli-Juuti, T.; Pajunoja, A.; Tikkanen, O.-P.; Buchholz, A.; Faiola, C.; Väisänen, O.; Hao, L.; Kari, E.; Peräkylä, O.; Garmash, O.; Shiraiwa, M.; Ehn, M.; Lehtinen, K.; Virtanen, A. Factors Controlling the Evaporation of Secondary Organic Aerosol from α-Pinene Ozonolysis. *Geophys. Res. Lett.* **2017**, *44* (5), 2562–2570. https://doi.org/10.1002/2016GL072364.

(108)   Wall, A. C. V.; Perraud, V.; Wingen, L. M.; Finlayson-Pitts, B. J. Evidence for a Kinetically Controlled Burying Mechanism for Growth of High Viscosity Secondary Organic Aerosol. *Environ. Sci. Process. Impacts* **2020**, *22* (1), 66–83. https://doi.org/10.1039/C9EM00379G.

(109)   Wolf, M. J.; Zhang, Y.; Zawadowicz, M. A.; Goodell, M.; Froyd, K.; Freney, E.; Sellegri, K.; Rösch, M.; Cui, T.; Winter, M.; Lacher, L.; Axisa, D.; DeMott, P. J.; Levin, E. J. T.; Gute, E.; Abbatt, J.; Koss, A.; Kroll, J. H.; Surratt, J. D.; Cziczo, D. J. A Biogenic Secondary Organic Aerosol Source of Cirrus Ice Nucleating Particles. *Nat. Commun.* **2020**, *11* (1). https://doi.org/10.1038/s41467-020-18424-6.

(110)   Murray, B. J.; Wilson, T. W.; Dobbie, S.; Cui, Z.; Al-Jumur, S. M. R. K.; Möhler, O.; Schnaiter, M.; Wagner, R.; Benz, S.; Niemand, M.; Saathoff, H.; Ebert, V.; Wagner, S.; Kärcher, B. Heterogeneous Nucleation of Ice Particles on Glassy Aerosols under Cirrus Conditions. *Nat. Geosci.* **2010**, *3* (4), 233–237. https://doi.org/10.1038/ngeo817.

(111)   Schill, G. P.; Tolbert, M. A. Heterogeneous Ice Nucleation on Phase-Separated Organic-Sulfate Particles: Effect of Liquid vs. Glassy Coatings. *Atmospheric Chem. Phys.* **2013**, *13* (9), 4681–4695. https://doi.org/10.5194/acp-13-4681-2013.

(112)   Ignatius, K.; Kristensen, T. B.; Järvinen, E.; Nichman, L.; Fuchs, C.; Gordon, H.; Herenz, P.; Hoyle, C. R.; Duplissy, J.; Garimella, S.; Dias, A.; Frege, C.; Höppel, N.; Tröstl, J.; Wagner, R.; Yan, C.; Amorim, A.; Baltensperger, U.; Curtius, J.; Donahue, N. M.; Gallagher, M. W.; Kirkby, J.; Kulmala, M.; Möhler, O.; Saathoff, H.; Schnaiter, M.; Tomé, A.; Virtanen, A.; Worsnop, D.; Stratmann, F. Heterogeneous Ice Nucleation of Viscous Secondary Organic Aerosol Produced from Ozonolysis of α-Pinene. *Atmospheric Chem. Phys.* **2016**, *16* (10), 6495–6509. https://doi.org/10.5194/acp-16-6495-2016.

(113)   James, A. D.; Brooke, J. S. A.; Mangan, T. P.; Whale, T. F.; Plane, J. M. C.; Murray, B. J. Nucleation of Nitric Acid Hydrates in Polar Stratospheric Clouds by Meteoric Material. *Atmospheric Chem. Phys.* **2018**, *18* (7), 4519–4531. https://doi.org/10.5194/acp-18-4519-2018.

(114)   Barry, K. R.; Hill, T. C. J.; Levin, E. J. T.; Twohy, C. H.; Moore, K. A.; Weller, Z. D.; Toohey, D. W.; Reeves, M.; Campos, T.; Geiss, R.; Schill, G. P.; Fischer, E. V.; Kreidenweis, S. M.; DeMott, P. J. Observations of Ice Nucleating Particles in the Free Troposphere From Western US Wildfires. *J. Geophys. Res. Atmospheres* **2021**, *126* (3), 1–17. https://doi.org/10.1029/2020JD033752.

(115)   Kasparoglu, S.; Perkins, R.; Ziemann, P. J.; DeMott, P. J.; Kreidenweis, S. M.; Finewax, Z.; Deming, B. L.; DeVault, M. P.; Petters, M. D. Experimental Determination of the Relationship Between Organic Aerosol Viscosity and Ice Nucleation at Upper Free Tropospheric Conditions. *J. Geophys. Res. Atmospheres* **2022**, *127* (16), e2021JD036296. https://doi.org/10.1029/2021JD036296.

(116)   Jahn, L. G.; Polen, M. J.; Jahl, L. G.; Brubaker, T. A.; Somers, J.; Sullivan, R. C. Biomass Combustion Produces Ice-Active Minerals in Biomass-Burning Aerosol and Bottom Ash. *Proc. Natl. Acad. Sci. U. S. A.* **2020**, *117* (36), 21928–21937. https://doi.org/10.1073/pnas.1922128117.

(117)   Petters, M. D.; Parsons, M. T.; Prenni, A. J.; Demott, P. J.; Kreidenweis, S. M.; Carrico, C. M.; Sullivan, A. P.; McMeeking, G. R.; Levin, E.; Wold, C. E.; Collett, J. L.; Moosmüller, H. Ice Nuclei Emissions from Biomass Burning. *J. Geophys. Res. Atmospheres* **2009**, *114* (7), 1–10. https://doi.org/10.1029/2008JD011532.

(118)   Altaf, M. B.; Freedman, M. A. Effect of Drying Rate on Aerosol Particle Morphology. *J Phys Chem Lett* **2017**, *8* (15), 3613–3618. https://doi.org/10.1021/acs.jpclett.7b01327.

(119)   Petters, M.; Kasparoglu, S. Predicting the Influence of Particle Size on the Glass Transition Temperature and Viscosity of Secondary Organic Material. *Sci. Rep.* **2020**, *10* (1). https://doi.org/10.1038/s41598-020-71490-0.

(120)   Shi, S.; Cheng, T.; Gu, X.; Guo, H.; Wu, Y.; Wang, Y. Biomass Burning Aerosol Characteristics for Different Vegetation Types in Different Aging Periods. *Environ. Int.* **2019**, *126* (October 2018), 504–511. https://doi.org/10.1016/j.envint.2019.02.073.

(121)   Yu, X.; Shi, C.; Ma, J.; Zhu, B.; Li, M.; Wang, J.; Yang, S.; Kang, N. Aerosol Optical Properties during Firework, Biomass Burning and Dust Episodes in Beijing. *Atmos. Environ.* **2013**, *81*, 475–484. https://doi.org/10.1016/j.atmosenv.2013.08.067.

(122)   Ogunjobi, K. O.; He, Z.; Kim, K. W.; Kim, Y. J. Aerosol Optical Depth during Episodes of Asian Dust Storms and Biomass Burning at Kwangju, South Korea. *Atmos. Environ.* **2004**, *38* (9), 1313–1323. https://doi.org/10.1016/j.atmosenv.2003.11.031.

For Table of Contents Only